ACS APPLIED ENERGY MATERIALS

www.acsaem.org Article

An Efficient Copper-Based Redox Shuttle Bearing a Hexadentate Polypyridyl Ligand for DSCs under Low-Light Conditions

Anthony Devdass, Jonathon Watson, Eric Firestone, Thomas W. Hamann,* Jared H. Delcamp,* and Jonah W. Jurss*

Cite This: *ACS Appl. Energy Mater.* 2022, 5, 5964−5973 Read Online

ACCESS | Metrics & More | Article Recommendations | Supporting Information

ABSTRACT: A Cu complex featuring a hexadentate ligand was synthesized and evaluated as a redox shuttle in dye-sensitized solar cell (DSC) devices, which exhibited excellent performance under low-light conditions. Cu-based redox shuttles (RSs) have been shown to perform remarkably well under low-light conditions; however, most of the known Cu-based RSs employ bidentate pyridyl ligands and often require bulky flanking groups adjacent to the nitrogen donors of these ligands to prevent distortion and binding of exogenous Lewis bases such as 4-*tert*-butylpyridine (TBP) that are added to enhance cell performance. Without the bulky substituents, the bidentate ligands are susceptible to ligand exchange with TBP. In this context, we have developed a Cu-based RS with a preorganized multidentate ligand designed to facilitate efficient electron transfer kinetics and high stability via the chelate effect. The Cu system, $[Cu(bpyPY4)]^{2+/+}$, reported here is supported by the hexadentate polypyridyl ligand bpyPY4 (6,6′-bis(1,1-di(pyridine-2-yl)ethyl)-2,2′-bipyridine) and examined as a RS in DSCs. From X-ray crystallography and variable-temperature ^{1}H NMR studies, bpyPY4 provides a dynamic coordination environment around the metal center. Cyclic voltammetry and UV−visible and NMR spectroscopy indicate that noncoordinated pyridyl donors block binding of TBP to copper. DSC devices using $[Cu(bpyPY4)]^{2+/+}$ as the redox electrolyte gave a power conversion efficiency (PCE) value of 4.9% under 1 sun illumination (100 mW/cm^2). Strikingly, the device performance increased to 11.11% when irradiated with 2400 lux (0.5 mW/cm^2) via a fluorescent lamp light source and improved further to 15.2% PCE at 13500 lux (2.10 mW/cm^2). The Cu redox shuttle is an intriguing candidate for implementation with narrow band gap sensitizers with low oxidation potentials, which are important for high photocurrent DSC devices.

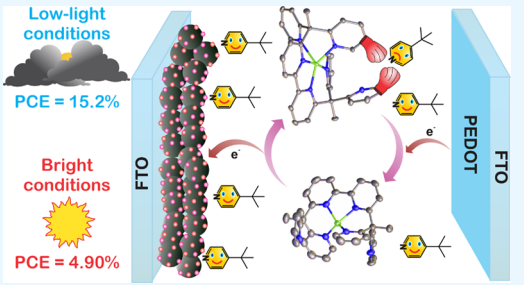

KEYWORDS: *hexadentate polypyridyl ligand, low-light conditions, copper-based redox shuttle, dye-sensitized solar cells, dynamic, fluxional coordination behavior, electron transfer kinetics*

INTRODUCTION

The need to generate carbon neutral energy has led to the development of new technologies that utilize renewable sources such as wind and solar energy.[1,2] Photovoltaic cells are capable of harnessing sunlight for solar-to-electrical energy conversion.[3−5] Dye-sensitized solar cells (DSCs) serve as an attractive photovoltaic technology, which are inexpensive and have high photon-to-current conversion efficiencies under all lighting conditions.[6−11] A DSC is composed of a chromophore anchored to a semiconducting mesoporous metal oxide surface, which upon photoexcitation, injects an electron into the conduction band of the semiconductor. The oxidized chromophore (or dye) is then reduced back to its initial state by a redox shuttle (RS) in the solution, a process known as regeneration. The injected electron then traverses an external circuit to the counter electrode, where the oxidized redox shuttle is reduced to complete the circuit.[5,6,12] The classically used iodide/triiodide (I^-/I_3^-) RS system has several shortcomings such as its corrosive nature, lack of tunability, competitive absorption in the visible region by the triiodide ion, and a two-electron redox couple that results in significant energy losses.[13−16]

Transition metal complexes have been proven to be a successful replacement for the I^-/I_3^- redox couple where the solar-to-electric power conversion efficiencies (PCEs) have increased from 11% for I^-/I_3^- to >14% for $Co^{III/II}$-based RSs.[17−23] Inspired by copper-containing metalloenzymes known as blue copper proteins, which are capable of highly efficient single-electron transfer reactions,[24−26] Fukuzumi and co-workers tested model copper complexes as RSs for the first time in DSCs.[27] Following this study, a number of Cu-based RSs have been developed, exhibiting significant improvements in terms of efficiency.[10,28−49] Cu-based RSs have also been

Received: January 31, 2022
Accepted: April 18, 2022
Published: May 4, 2022

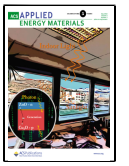

https://doi.org/10.1021/acsaem.2c00344
ACS Appl. Energy Mater. 2022, 5, 5964−5973

successfully employed as hole transport materials (HTMs) in solid-state DSCs with impressive PCE values.[10,28,35] Recently, DSCs with Cu-based RSs have been shown to perform exceptionally well under ambient light conditions, thus making it a promising technology for indoor applications such as sensors, wearable devices, and autonomous Internet of Things (IoT) devices.[9,10,50−52] An initial report on the cosensitization of dyes in conjunction with a Cu-based RS in DSCs, as a strategy to achieve better efficiencies, led to high open circuit voltages (V_{OC}) of up to 1.1 V with a PCE of 28.9% at 1000 lux intensity under ambient light conditions.[9] Later, an exceptional V_{OC} of 1.24 V with a different set of cosensitized dyes in association with a Cu-based RS set a record PCE of 34.5% at 1000 lux intensity under fluorescent lighting.[53]

The I^-/I_3^- redox couple involves an overall two-electron redox process that typically results in a lower theoretical maximum photovoltage output from DSC devices relative to one-electron redox processes.[16,29] On the other hand, $Co^{III/II}$-based RSs present a challenge where a large inner-sphere reorganization energy is often associated with the electron transfer process in going from a high spin, d^7 (Co^{II}) system to a low spin, d^6 (Co^{III}) system.[54,55] This affects the kinetics of dye regeneration as the available driving force for electron transfer is limited.[29] Indeed, Cu-based RSs have been proven to be on par with the classical I^-/I_3^- and $Co^{III/II}$-based RSs, which has been possible due to their lower inner-sphere electron transfer reorganization energies.[33,44,56] Copper complexes are known to adopt multiple geometries based on the metal oxidation state and ligand environment. Cu^{II} (d^9) complexes often feature six-coordinate (octahedral or tetragonal), five-coordinate (square pyramidal or trigonal bipyramidal), or four-coordinate (tetrahedral or square planar) geometries.[24,57] Similarly, Cu^{I} (d^{10}) complexes usually attain four-coordinate (tetrahedral) geometries.[26] Most Cu RSs used in DSCs to-date employ bidentate bipyridine or phenanthroline[28]-based ligands with bulky groups flanking the nitrogen donors in order to minimize structural changes between the Cu^{II} and Cu^{I} redox states. Freitag and co-workers introduced a tetradentate $Cu^{II/I}$ redox shuttle in DSCs that was found to have high stability due to the chelate effect and lower photovoltage losses (V_{OC}^{loss}) arising from a lower inner-sphere reorganization energy for electron transfer.[37] We recently reported $Cu^{II/I}$ RSs with rigid tetradentate ligands that promoted lower inner-sphere reorganization energies leading to improved short-circuit current densities (J_{SC}), high stability, and a decrease in V_{OC}^{loss}.[44]

Cu-based RSs bearing pentadentate ligands were recently employed in DSC devices by Sun and co-workers.[58] The advantage of having a pentadentate Cu^{II} complex and its effect on the coordination of commonly used Lewis base additive 4-*tert*-butylpyridine (TBP) was investigated. Exceptional long-term stability was observed with DSC devices using the $[Cu(tme)]^{2+/+}$ (tme = *N*-benzyl-*N*,*N*′,*N*′-tris(6-methylpyridin-2-ylmethyl)ehtylenediamine) RS, and added TBP was shown to not bind to $[Cu(tme)]^{2+}$.[58] We have been focused on developing Cu-based RSs supported by preorganized multidentate ligands to facilitate efficient electron transfer kinetics and high stability in DSCs.[44] Herein, we report the implementation of a Cu(II/I) redox system bearing a hexadentate polypyridyl ligand (6,6′-bis(1,1-di(pyridine-2-yl)-ethyl)-2,2′-bipyridine, bpyPY4) as a RS in DSCs.

RESULTS AND DISCUSSION

Synthesis and Characterization. The synthesis of the ligand, bpyPY4, has been previously reported,[59] where 1,1-bis(2-pyridyl)ethane[60] is deprotonated using *n*-BuLi followed by addition of the electrophile, 6,6′-dibromo-2,2′-bipyridine.[61] The metalation is carried out using an equimolar ratio of the appropriate Cu salt (either $[Cu(CH_3CN)_4](PF_6)$ or $Cu(OTf)_2$ where OTf = trifluoromethanesulfonate) with bpyPY4 in acetonitrile (CH_3CN) to afford $[Cu(bpyPY4)](PF_6)$ or $[Cu(bpyPY4)](OTf)_2$, respectively. The complexes were purified by slow diffusion of diethyl ether into concentrated CH_3CN solutions and characterized by ^1H and $^{13}C\{^1H\}$ NMR spectroscopy (Figures S1−S4) and high-resolution mass spectrometry.

Solid-state structures of the Cu complexes were determined by single crystal X-ray diffraction. Thermal ellipsoid plots of the cations are shown in Scheme 1. Crystal structure

Scheme 1. Syntheses of the $[Cu(bpyPY4)]^{2+/+}$ Complexes and Crystal Structures of the Cations of the Cu^I Species (Left) and Cu^{II} Species (Right) with Thermal Ellipsoids Shown at the 50% Probability Level[a]

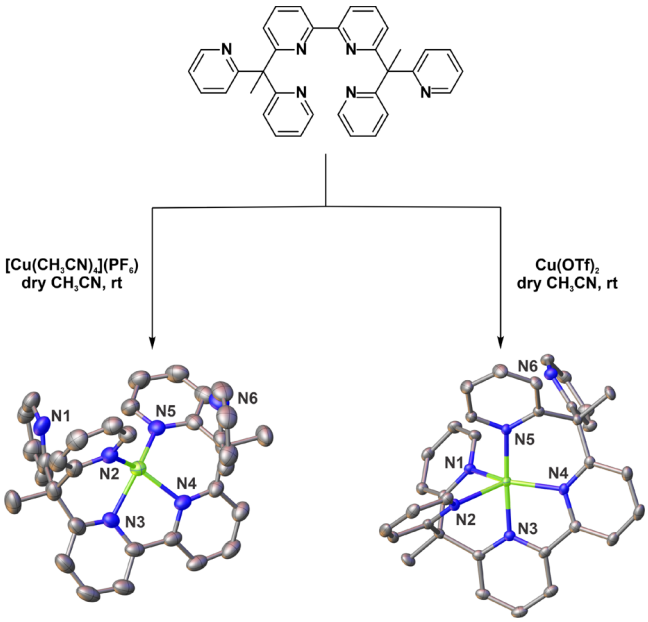

[a]Hydrogen atoms have been omitted for clarity.

information and refinement parameters are provided in Table S1. The hexadentate ligand enforces a five-coordinate geometry around the Cu^{II} center with five of the six pyridine donors of the bpyPY4 scaffold bound to copper. In contrast, a four-coordinate geometry is enforced around the Cu^{I} center where two of the pyridine donors of bpyPY4 are not bound to the metal. Geometric indices, τ_5 and τ_4, have been developed for five-coordinate and four-coordinate complexes, respectively, to describe the degree of distortion between ideal geometries where the τ value in each case will range from 0 to 1.[62,63] For a five-coordinate complex, a τ_5 value of 0 is associated with an ideal square pyramidal geometry and a value of 1 denotes an ideal trigonal bipyramidal geometry.[62] The τ_5 value for the Cu^{II} complex is 0.62, which corresponds to a distorted trigonal bipyramidal geometry. The bipyridine (N_{bpy}) fragment of the κ^5-bpyPY4 ligand occupies both an axial and an

https://doi.org/10.1021/acsaem.2c00344
ACS Appl. Energy Mater. 2022, 5, 5964−5973

equatorial position around the Cu^{II} ion with the other sites occupied by pyridine (N_{py}) donors. The distortion in the five-coordinate Cu^{II} complex is apparent by the displacement of the Cu^{II} ion from the plane defined by the three equatorial donors. The Cu^{II} ion lies above the plane, toward the axial pyridine (N_{py}) donor (*trans* to the axial N-donor of the bipyridine group), at a displacement distance of 0.225 Å. The angles formed by the axial N_{py} donor, the Cu^{II} ion, and the equatorial donors are slightly greater than 90° due to the displacement of the Cu^{II} ion toward the apical pyridine donor. The bipyridine fragment has a nearly planar geometry and exhibits a torsion angle between its pyridine rings of −6.38°.

For a four-coordinate complex, an ideal square planar geometry has a τ_4 value of 0 and an ideal tetrahedral geometry has τ_4 = 1.[63] The Cu^{I} complex features a highly distorted tetrahedral geometry with a calculated τ_4 value of 0.63. The κ^4-bpyPY4 ligand binds the Cu^{I} ion with the bipyridine unit occupying two of the coordination sites, while the other two sites are occupied by one pyridine from each of the 1,1-bis(2-pyridyl)ethane fragments. The average Cu-N_{bpy} bond distance is 2.055(7) Å around the Cu^{I} ion and is comparable to other known tetrahedral Cu^{I} complexes bearing bipyridine ligands.[64−66] However, the average Cu-N_{py} bond distance is shorter in comparison at 1.990(2) Å. The bipyridyl group in this case exhibits significant distortion with a torsion angle between its pyridine rings of 19.73°.

The ^{1}H NMR spectrum of [Cu(bpyPY4)](PF_6) was recorded in CD_3CN at room temperature where 14 aromatic protons are observed following integration (Figure 1). Two

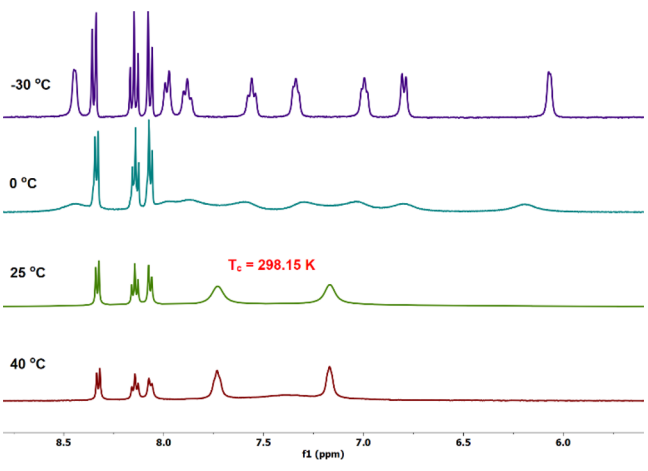

Figure 1. Variable temperature ^{1}H NMR spectra of $[Cu(bpyPY4)]^+$ in CD_3CN.

broad peaks of equal intensity are observed at δ = 7.17 and 7.73 ppm that integrate for a total of eight protons (four protons each). Sharp resonances, consisting of two doublets and a triplet, are observed further downfield in the aromatic region, which together integrate to six protons (two protons each) and correspond to the bipyridine unit. However, the bpyPY4 framework has 22 aromatic protons. As seen in the solid-state structure of the Cu^{I} complex (Scheme 1), two pyridines, accounting for eight aromatic protons, are not coordinated to the metal center. We reasoned that at room temperature, the two broad resonance peaks and the eight "missing" aromatic protons are due to rapid exchange on the NMR timescale between the noncoordinated and coordinated pyridine donors where the protons associated with the noncoordinated pyridines appear as a single broad peak at 7.17 ppm and those of the coordinated pyridines appear as a single broad peak at 7.73 ppm. To probe this hypothesis, variable-temperature ^{1}H NMR spectroscopy was performed. Spectra at temperatures ranging from −30 to 40 °C are stacked in Figure 1 and Figure S5 that confirm the dynamic coordination behavior in solution. Upon lowering the temperature, several broad resonance peaks begin to appear at 5 °C, and eight new broad peaks emerge where distinct peak splitting becomes apparent as the temperature reaches −30 °C. The eight new peaks integrate to a total of 16 protons (two protons each) and arise from the four terminal pyridines as shown in Figure S1. The eight chemically distinct signals are consistent with two different chemical environments for the exchanging pyridines. We hypothesize that two of the fluxional pyridines, one from each dipyridylethane "arm", are noncoordinated and in equivalent environments, each having four unique aromatic protons. Likewise, the other two pyridines are coordinated and chemically equivalent and account for the four remaining peaks. A ^{1}H-^{1}H 2D gradient-selected COSY (gCOSY) experiment was carried out at −30 °C to assign the chemical shifts arising from the coordinated and noncoordinated pyridines (Figure S3). Analysis of this spectrum confirms two sets of pyridine environments. The chemical shifts for the noncoordinated pyridines do not line up strictly with the free ligand, but similar studies have shown a downfield shift for dissociated heterocycles that are part of a coordinated ligand framework.[67,68] A free energy of activation ($\Delta G^{\ddagger}$) for the exchange process is estimated to be ∼14 kcal/mol; details of our analysis are provided in the Supporting Information.

The UV−visible−NIR spectra of the Cu complexes were recorded in anhydrous CH_3CN, and the molar absorptivities (ε) of the observed bands were determined by serial dilution (Figure S7). Intense absorption peaks in both complexes are observed at 193 nm followed by absorption bands of moderate intensity from 249 to 324 nm with molar absorptivities ranging from 22,700 to 11,400 M^{-1} cm^{-1}. Lower intensity shoulders are observed at 329, 391, and 450 nm for the Cu^{I} complex with molar absorptivities of 4260, 2920, and 1730 M^{-1} cm^{-1}, respectively. A small shoulder peak corresponding to a metal-to-ligand charge transfer (MLCT) band is observed at 538 nm (ε = 1000 M^{-1} cm^{-1}). The Cu^{II} complex exhibits two relatively weak bands corresponding to d−d transitions at 616 (ε = 152 M^{-1} cm^{-1}) and 845 nm (114 M^{-1} cm^{-1}), which are indicative of a structure that favors a square pyramidal geometry in solution.[69−72]

The redox properties of the Cu^{II} complex were then investigated by cyclic voltammetry. The cyclic voltammogram (CV) of the complex is shown in Figure S8, where a $Cu^{II/I}$ redox couple is observed at −0.43 V versus the ferrocenium/ferrocene ($Fc^{+/0}$) couple (0.21 V vs NHE).[73,74] The redox couple is fairly reversible with a peak splitting value of 90 mV. This redox potential is surprisingly negative relative to most previously reported $Cu^{II/I}$ redox couples. Rorabacher and co-workers showed that the potential of a $Cu^{II/I}$ redox couple is correlated with the stability of the Cu(II) form of the redox couple.[75] The relationship is Nernstian with a 0.059 V negative shift in potential for each 10-fold increase in the stability constant. Thus, the negative redox potential indicates a very stable Cu^{II} complex.

Lewis bases, such as TBP and *N*-methylbenzimidazole (NMBI), are frequently used as additives in DSC devices to enhance the overall cell performance.[76−78] The enhancement

https://doi.org/10.1021/acsaem.2c00344
ACS Appl. Energy Mater. 2022, 5, 5964−5973

observed with added Lewis bases is attributed to shifting the titania conduction band edge to more negative potentials and reducing the interfacial charge recombination rates by surface adsorption.[77,79−81] With most of the reported Cu-based RSs, TBP is known to coordinate with the Cu^{II} species and even displace polydentate ligands, which has a significant impact on the redox potential as multiple redox species are produced, affecting the maximum achievable photovoltage and electron transfer kinetics.[29,41,58,82−86] In this context, the effect of TBP on the $[Cu(bpyPY4)]^{2+/+}$ redox couple was evaluated in the presence of different concentrations of the Lewis base. TBP was added in excess of 10 equivalents relative to $[Cu(bpyPY4)]^{2+}$ in solution to match the conditions used in the devices described below. Importantly, the addition of TBP shows no significant influence on the $Cu^{II/I}$ redox couple (Figure S9). The effect of TBP was further evaluated using UV−vis spectroscopy where spectra were recorded as a function of added TBP (Figure S10). No significant change was observed in the UV−visible absorption spectra, confirming that TBP does not bind to the metal center of this RS. Finally, the effect of TBP was evaluated using ^1H NMR spectroscopy in which the $[Cu(bpyPY4)]^{2+}$ sample was titrated with TBP (Figure S11). As TBP was added, no signals associated with free bpyPY4 were observed, indicating that no ligand substitution occurs. The transient, noncoordinated, proximal pyridines of the hexadentate ligand presumably block any open coordination sites on the metal to avoid deleterious binding of exogenous Lewis bases. This finding is also in agreement with the very high stability of the Cu^{II} species indicated by the $Cu^{II/I}$ redox potential.

Stopped-flow spectroscopy was utilized to measure the cross-exchange electron transfer rate constant, k_{12}, between $[Cu(bpyPY4)]^{2+}$ and decamethylferrocene ($Fe(Cp^*)_2$). The stopped-flow measurements were carried out in the manner previously reported and detailed in the Supporting Information.[87] Following this method, the self-exchange rate for the $[Cu(bpyPY4)]^{2+/+}$ couple was determined to be 8.78 ± 0.96 M^{-1} s^{-1} (see Table S4). This self-exchange rate constant is surprisingly slow, which is due to a large inner-sphere reorganization energy, which was calculated to be approximately 1 eV per molecule (calculation detailed in the Supporting Information), due to the change in geometry and coordination number upon electron transfer as shown in Scheme 1.[88]

Photovoltaic Performance. DSC devices were fabricated with $[Cu(bpyPY4)]^{2+/+}$ as the RS in conjunction with a poly(3,4-ethylenedioxythiophene) (PEDOT) counter electrode and commercial dyes XY1b and Y123 as the cosensitized light-harvesting component (Figure S13). These sensitizers were selected due to a well-established record of efficient electricity generation and superior insulation of injected electrons in TiO_2 from the electrolyte.[10,35,53] Electrochemical investigation of the RS revealed favorable energetics for use with the XY1b/Y123 dye system with a high thermodynamic driving force of regeneration (ΔG_{reg}) in excess of 800 mV (Figure 3). The devices were characterized by current density versus voltage (J−V) analysis for determination of the PCE given by the equation: $PCE = (J_{SC} \times V_{OC} \times FF)/I_0$, where J_{SC} is the short-circuit density, FF is the fill factor, and I_0 is the incident light intensity set to 1 sun at AM1.5G (100 mW/cm^2) unless otherwise noted.

Devices constructed using the abovementioned materials gave respectable performance with a J_{SC} of 13.3 mA/cm^2 and an overall PCE of 4.9% (Table 1). The observed photocurrent is the result of panchromatic electricity generation from 400 to 650 nm as shown by the incident photon-to-current conversion efficiency (IPCE) spectrum, maintaining a peak IPCE value of ∼70% (Figure 4). In addition, the $[Cu(bpyPY4)]^{2+/+}$ RS shows negligible absorption in this region of the spectrum, therefore minimizing competitive light absorption between the sensitizers and RS (Figure 2).[89]

Table 1. Summary of DSC Device Performance Metrics

source	power (mW/cm^2) (lux)	V_{OC} (mV)	J_{SC} (mA/cm^2)	FF (%)	PCE (%)
AM1.5G	100	580	13.3	58.8	4.90
fluorescent	0.50 (2400)	406	0.221	62.2	11.1
fluorescent	1.44 (10000)	466	0.695	65.3	14.7
fluorescent	2.10 (13500)	485	1.001	65.4	15.2

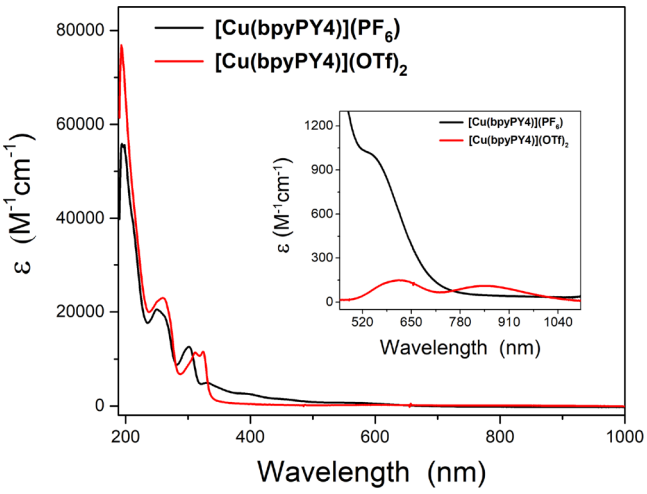

Figure 2. UV−visible−NIR spectra of the Cu redox shuttle in anhydrous CH_3CN.

The V_{OC} parameter is a key metric that is largely determined by semiconductor and RS selection. The maximum theoretical photovoltage (V_{OC}^{max}) for DSC devices is defined as the energetic difference between the semiconductor (TiO_2) conduction band and the RS oxidation potential. Taking the TiO_2 CB to be the commonly used value in the literature of −0.5 V versus NHE,[5,90,91] then the V_{OC}^{max} for the system in this study is 710 mV. An observed photovoltage (V_{OC}^{obs}) of 580 mV was obtained for these devices, which corresponds to a photovoltage loss (V_{OC}^{loss}) of only 130 mV according to the equation $V_{OC}^{loss} = V_{OC}^{max} - V_{OC}^{obs}$ if no shift in the TiO_2 CB has occurred. A small V_{OC}^{loss} is possible when minimal recombination loss from electrons in TiO_2 with the electrolyte is present. Low V_{OC}^{loss} values have also been correlated to small inner-sphere electron transfer reorganization energies as pointed out in earlier work involving Cu-based redox shuttles supported by multidentate ligands.[37,44]

Electrochemical impedance spectroscopy (EIS) measurements were subsequently performed in the dark at an applied potential of 580 mV (which corresponds to open circuit potential under illumination) in order to further investigate the recombination pathway. The data was fitted using a template circuit and then used to generate the Nyquist and Bode plots (Figure 5 and Figure S14). Charge transfer resistance at the

https://doi.org/10.1021/acsaem.2c00344
ACS Appl. Energy Mater. 2022, 5, 5964−5973

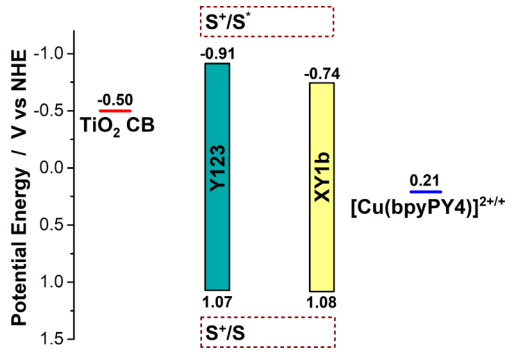

Figure 3. Energy level diagram of dyes Y123 and XY1b, $[Cu(bpyPY4)]^{2+/+}$, and the TiO_2 conduction band.

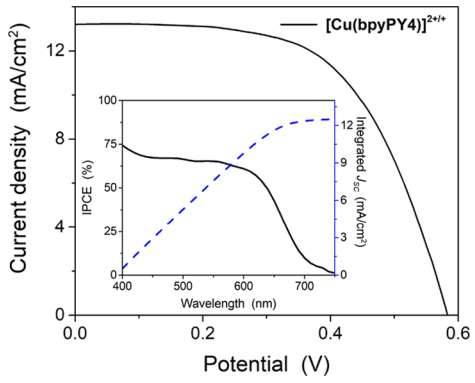

Figure 4. $J-V$ and IPCE (inset) curves for the $[Cu(bpyPY4)]^{2+/+}$-based DSC devices. For the IPCE, the solid black line is the IPCE response and the dashed blue line represents the integrated photocurrent.

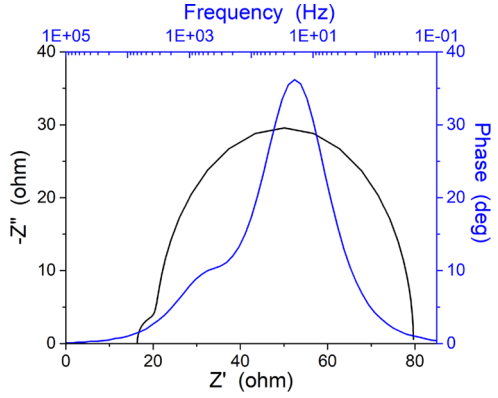

Figure 5. EIS data for DSC devices. The Nyquist (primary axis, black) and Bode (secondary axis, blue) plots are shown. The small semicircle in the Nyquist plot represents R_{CE}, while the large semicircle corresponds to R_{rec}.

counter electrode (R_{CE}) was low with the PEDOT counter electrodes used here at 4 Ω, which indicates that PEDOT is a suitable counter electrode for use with the $[Cu(bpyPY4)]^{2+/+}$ redox shuttle. Resistance at the TiO_2-dye-electrolyte interface (R_{rec}) is desirably higher for a functional DSC device at 59 Ω. From the fitted circuit (Figure S14), the lifetime of electrons in TiO_2 (τ_{TiO_2}) was calculated to be 16 ms according to the equation $\tau_{TiO_2} = R_{rec} \times C_\mu$, where C_μ is the capacitance at the TiO_2-dye-electrolyte interface (Figure 5 and Table S5). Photocurrent dynamics measurements conducted by shutter-ing varied irradiation intensities on and off were performed (Figure S15). These studies reveal inadequate electrolyte diffusion rates at 1 sun intensity (100 mW/cm^2) to sustain the initial current flow as the shutter opens, which is seen as a sharp spike in the photocurrent response before the equilibrium is reached at higher light intensities. At approximately 50 mW/cm^2 (0.50 sun intensity), the diffusion rate of the electrolyte is adequate for transporting charge without current limitations as no spike upon shutter opening is observed. This suggests more efficient use of photons at lower light intensities, which is consistent with reported observations of other Cu-based redox shuttle systems.[29,36] Notably, diffusion limits or mass transport limits at higher light intensities have been noted in the literature with high light intensities and Cu-based redox shuttles.[36,92] The $[Cu(bpyPY4)]^{2+/+}$ redox shuttle has a notable spike in current, visible as low as 79% of AM1.5G intensity (79 mW/cm^2). This may be due in part to a non-Cu coordinating pyridine group binding to TiO_2 limiting the mass transport rate. The RS was also tested as a solid-state hole transporting material by slow evaporation of the electrolyte solvent under inert (glovebox) and ambient conditions. Solar cells fabricated under these conditions resulted in nonoperative devices. This observation is consistent with the slow self-exchange kinetics.[93]

DSC devices are well known in the literature for enhanced performance under reduced illumination intensities making them suitable for indoor lighting applications. Indoor/ambient lighting characterization was performed by $J-V$ analysis using an Osram 011318-L36W/930 fluorescent tube as the illumination source as has been used in the literature.[9] The light intensity was determined prior to each measurement using a digital lux meter in combination with a solar power meter and varied by changing the distance between the light source and the device under study. The $J-V$ plots for devices measured at 2400, 10000, and 13500 lux are presented in Figure 6 and tabulated in Table 1 and Table S6. Under 2400

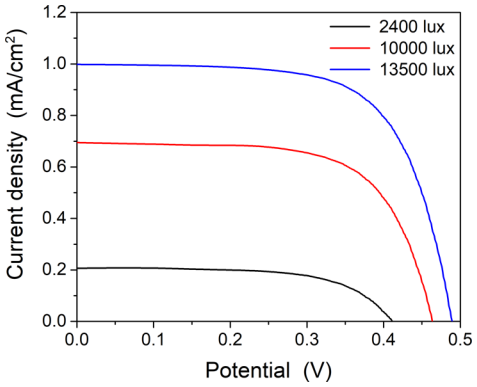

Figure 6. $J-V$ curves for DSC devices under fluorescent lighting.

lux illumination, the $[Cu(bpyPY4)]^{2+/+}$-based devices reached a PCE of 11.1 ± 0.8%. The observed PCE corresponds to device output power (P_{out}) = 55.5 μW/cm^2, V_{OC} = 406 ± 9 mV, J_{SC} = 221 ± 19 μA/cm^2, and FF = 62.2 ± 0.4%. Increasing the intensity of the incident fluorescent lighting to 13500 lux resulted in better performing devices, reaching a maximum PCE of 15.2% with P_{out} = 319 μW/cm^2, V_{OC} = 485 mV, J_{SC} = 1006 μA/cm^2, and FF = 65.4% (champion cell PCE of 15.5%). The high performance under fluorescent lighting illustrates the

https://doi.org/10.1021/acsaem.2c00344
ACS Appl. Energy Mater. 2022, 5, 5964−5973

importance of RSs such as the hexadentate Cu redox couple presented here.

CONCLUSIONS

We have developed a copper-based redox shuttle bearing a hexadentate polypyridyl ligand, bpyPY4, and applied it to cosensitized DSCs using commercial benchmark dyes XY1b and Y123. The experimental results indicate that the transient, noncoordinated, proximal pyridines of the hexadentate ligand prevent coordination of TBP, a common additive in efficient DSC devices. The self-exchange rate constant for $[Cu(bpyPY4)]^{2+/+}$ was evaluated using stopped-flow spectroscopy, and the results suggest a slower electron transfer rate due to high inner-sphere electron transfer reorganization energy. DSC devices fabricated using $[Cu(bpyPY4)]^{2+/+}$ as the electrolyte gave a PCE of 4.9% (~70% peak IPCE) as a result of efficient photogenerated electricity and minimal energy losses with a low-potential redox shuttle. We note that the hexadentate Cu RS was not suitable as a solid-state hole transporting material under the conditions tested. A unique advantage of DSCs over traditional photovoltaic technologies is enhanced performance under low-light illumination. Indeed, device metrics increased dramatically when irradiated with a fluorescent lamp light source compared to 1 sun illumination. This resulted in a PCE improvement from 4.9% at 1 sun (100 mW/cm^2 solar simulated spectrum) to 15.2% at 13500 lux with a fluorescent light source. Given the relatively low oxidation potential of the Cu RS, this RS is a suitable candidate for implementation with narrow band gap sensitizers for high photocurrent DSC devices. Future studies will focus on coupling this RS with NIR absorbing sensitizers and developing new hexadentate ligand designs to vary the energetics of the Cu species.

EXPERIMENTAL SECTION

Materials and Methods. Unless otherwise stated, all synthetic manipulations were carried out under an inert atmosphere using Schlenk techniques or in an MBraun glovebox under an nitrogen atmosphere. Acetonitrile (CH_3CN) used for synthesis and electrochemistry was freshly distilled from CaH_2 and stored over molecular sieves under an inert atmosphere. Tetrahydrofuran (THF) and diethyl ether used for synthesis were dried using a Pure Process Technology solvent purification system. Compounds were obtained from the following sources: 2,6-dibromopyridine from OxyChem, 2-fluoropyridine from Chem-Impex International, 2-ethylpyridine from Alfa Aesar, tetrakis(acetonitrile)copper(I) hexafluorophosphate ($[Cu(CH_3CN)_4]PF_6$) from TCI, anhydrous copper(II) chloride ($CuCl_2$) from Strem Chemicals, and *n*-butyllithium (2.3 M solution) from Acros Organics. All commercially obtained chemicals were used without further purification. ^1H and ^{13}C NMR spectra were recorded on a Bruker Ascend-400 NMR spectrometer and the obtained spectra were calibrated to residual protiated solvent peaks with chemical shifts reported in parts per million (ppm). The ^1H-^1H 2D gradient-selected COSY (gCOSY) experiment was obtained at −30 °C on a Bruker Ascend-400 spectrometer. The variable temperature NMR studies were performed on a Bruker Avance III HD 500 MHz spectrometer equipped with a 5 mm Prodigy H/F-BBO cryoprobe, BCU-I temperature controller. High-resolution electrospray ionization mass spectra (HR-ESI-MS) were obtained with a Waters SYNAPT XS mass spectrometer utilizing nanospray ionization. UV−visible spectra were recorded on an Agilent/Hewlett-Packard 8453 UV−vis spectrophotometer.

X-ray Crystallography. Single crystals of $[Cu(bpyPY4)](OTf)_2$ and $[Cu(bpyPY4)](PF_6)$ were secured to a fiber loop micromount and transferred to the goniometer head of a Bruker APEX-II CCD diffractometer or a Bruker Quest diffractometer, respectively. Both instruments were equipped with an Oxford Cryosystems low-temperature device. Examination and data collection were performed with Cu Kα radiation (λ = 1.54178 Å) at 173 K for $[Cu(bpyPY4)](OTf)_2$ or at 150 K for $[Cu(bpyPY4)](PF_6)$. Data was collected, reflections were indexed and processed, and the files were scaled and corrected for absorption using APEX3.[94] The space group was assigned, and the structure was solved by direct methods using XPREP within the SHELXTL suite of programs[95,96] and refined by full matrix least squares against F^2 with all reflections using Shelxl2018[97,98] and the graphical interface Shelxle.[99] All non-hydrogen atoms were refined anisotropically. Additional data collection and refinement details can be found in Table S1.

The crystallographic data have been deposited with the Cambridge Crystallographic Data Centre in the CIF format. CCDC 1976837 ($[Cu(bpyPY4)](OTf)_2$) and 2145397 ($[Cu(bpyPY4)](PF_6)$) contain the supplementary crystallographic data for this work. These data can be obtained free of charge from The Cambridge Crystallographic Data Centre via www.ccdc.cam.ac.uk/data_request/cif.

Electrochemical Measurements. Electrochemical measurements were performed using a Bioanalytical Systems, Inc. (BASi), Epsilon potentiostat. Cyclic voltammetry studies were carried out using a typical three-electrode set-up equipped with a glassy carbon disk working electrode (3 mm diameter, CH Instruments), a platinum wire counter electrode, and a silver wire quasi-reference electrode, which was referenced versus ferrocene as an internal standard at the end of experiments, where $Fc^{+/0}$ = 0.64 V vs NHE.[73,74] Anhydrous CH_3CN containing 0.1 M tetra-*n*-butylammonium hexafluorophosphate (Bu_4NPF_6) as the supporting electrolyte was used for electrochemical studies.

Synthesis. Starting materials 1,1-bis(2-pyridyl)ethane[60] and 6,6′-dibromo-2,2′-bipyridine[61] and the final ligand, bpyPY4, were synthesized according to published procedures.[59]

[Cu(bpyPY4)](OTf)$_2$. A mixture of bpyPY4 (100 mg, 0.19 mmol) and $Cu(OTf)_2$ (68.7 mg, 0.19 mmol) were dissolved in anhydrous CH_3CN (5 mL) and stirred overnight at room temperature. The solution was concentrated under reduced pressure, and the complex was precipitated from solution with the addition of diethyl ether. The pure complex was obtained by crystallization. Single crystals were grown by slow diffusion of diethyl ether into a concentrated CH_3CN solution. Yield = 114 mg (67%). Elem. Anal. calc. for $C_{36}H_{28}N_6F_6O_6S_2Cu$: C, 49.01; H, 3.20; N, 9.53. Found: C, 48.76; H, 3.23; N, 9.41. HR-ESI-MS *m*/*z* calc. for $[Cu(bpyPY4) + (OTf)]^+$, 732.1292; found, 732.1092.

[Cu(bpyPY4)](PF$_6$). Anhydrous CH_3CN (5 mL) was added to a mixture of bpyPY4 (100 mg, 0.19 mmol) and $[Cu(CH_3CN)_4](PF_6)$ (70.8 mg, 0.19 mmol) inside a glovebox, and the resulting solution was stirred overnight at room temperature. The solution was concentrated under reduced pressure before diethyl ether was added to induce precipitation of the complex. Pure complex was obtained by crystallization. Single crystals were grown by slow diffusion of diethyl ether into a concentrated CH_3CN solution. Yield = 108 mg (77%). ^1H NMR (400 MHz, CD_3CN): δ = 8.44 (d, *J* = 4.8 Hz, 2H), 8.35 (d, *J* = 7.9 Hz, 2H), 8.15 (t, *J* = 7.8 Hz, 2H), 8.07 (d, *J* = 8.0 Hz, 2H), 7.98 (d, *J* = 8.2 Hz, 2H), 7.88 (t, *J* = 8.0 Hz, 2H), 7.56 (t, *J* = 8.0 Hz, 2H), 7.34 (t, *J* = 7.2 Hz, 2H), 7.00 (t, *J* = 6.3 Hz, 2H), 6.80 (d, *J* = 8.0 Hz, 2H), 6.07 (d, *J* = 4.3 Hz, 2H), 2.20 (s, 6H). $^{13}C\{^1H\}$ NMR (75 MHz, CD_3CN): δ = 157.91, 151.80, 150.55, 138.74, 138.33, 125.07, 124.78, 123.26, 122.24, 59.51, 28.34, 1.27. HR-ESI-MS *m*/*z* calc. for $[Cu(bpyPY4)]^+$, 583.1771; found, 583.1768.

Cross-Exchange Kinetics Measurements. The cross-exchange kinetics measurements were carried out using stopped-flow spectroscopy. The stopped-flow measurements were performed in a manner previously reported.[87] Briefly, an Olis RSM 1000 DeSa rapid-scanning spectrophotometer containing a dual-beam UV−vis was used, which recorded to Olis SpectralWorks software. The instrument contained a quartz cell with a 1 cm path length. The analyzed sample was scanned every millisecond at 1 nm resolution. The 150 W xenon arc lamp was controlled using an LPS-220B lamp power supply and held to within 80−83 W during each measurement. The temperature was held at 25 ± 0.1 °C using a NESLAB RTE-140 chiller/circulator. The

https://doi.org/10.1021/acsaem.2c00344
ACS Appl. Energy Mater. 2022, 5, 5964−5973

$[Cu(bpyPY4)](TFSI)_2$ and $[Fe(Cp^*)_2]$ solutions were made neat using dry acetonitrile. A 10-fold excess of $[Fe(Cp^*)_2]$ was used to maintain pseudo-first-order conditions. The spectra were monitored at 450 nm to follow the growth of the Cu(I) species. The reactant concentrations are listed in the Supporting Information (see Table S2). Scientific Data Analysis Software was used to provide fits for the resulting observed pseudo-first-order rate constants, k_{obs}, using a nonlinear least-squares regression. Twelve independent trials were averaged to provide the measured k_{obs} values. Absorbance plots for each pseudo-first-order reaction were fit using $A = A_\infty + (A_0 - A_\infty)e^{-k_{obs}t}$. The error in the k_{obs} values was taken to be the standard deviation of the independent trials. The minimal error in concentration was propagated based on prepared stock solutions of each reaction mixture. It is assumed that efficient mixing leads to minimal deviations in the initial concentrations of the reactants.

Device Fabrication. DSC devices were prepared as previously described in the literature.[100] Chenodeoxycholic acid (CDCA) was used as purchased from Chem-Impex International. TEC 10 glass was used for the photoanode, and TEC 7 glass was used for the counter electrode (Hartford Glass). The photoanode consists of a 3 μm mesoporous TiO_2 active layer (particle size, 30 nm, Greatcell Solar, 30NR-D) and a 5.0 μm TiO_2 scattering layer (particle size, 100 nm, Solaronix R/SP). Sensitizing dyes XY1b (Dyenamo, batch L9M2) and Y123 (Dyenamo, batch M2M5) were used as purchased. The working photoanode was prepared by immersing the TiO_2 film into a XY1b/Y123 cocktail dye solution for 16 h. The cocktail dye solution was prepared by first making two separate solutions: a XY1b solution at 0.2 mM dye and 5 mM CDCA in 4:1 ethanol/tetrahydrofuran solvent combination and a Y123 solution at 0.2 mM dye in a 1:1 acetonitrile/*tert*-butanol solvent mixture. The final sensitizing cocktail solution was prepared by mixing both dye solutions in a 1:1 ratio (v/v). The electrolytes were 0.2 M Cu^I, 0.06 M Cu^{II}, 0.6 M TBP (4-*tert*-butylpyridine), and 0.1 M LiTFSI (lithium bis-(trifluoromethanesulfonyl)imide) in acetonitrile solvent. PEDOT (poly(3,4-ethylenedioxythiophene)) counter electrodes were prepared following the literature procedure and utilized for all devices in this study.[101] DSC cell measurements were conducted as previously reported.[100] *J*–*V* curves were generated utilizing masked solar cells with a circular active area of 0.1496 cm^2. For low light studies, an Osram lamp (model 011318-L36W/930) was used as the illumination source. A digital lux meter (Dr. Meter model no. LX1330B) was used in combination with an Amprobe solar power meter (Solar-100) in order to quantify incident light intensity for low light studies.

■ ASSOCIATED CONTENT

Supporting Information

The Supporting Information is available free of charge at https://pubs.acs.org/doi/10.1021/acsaem.2c00344.

Characterization of the copper compounds; crystal data and refinement details; electrochemical, UV–vis, and variable-temperature NMR results; details of cross-exchange kinetics calculations; and DSC device data (PDF)

■ AUTHOR INFORMATION

Corresponding Authors

Thomas W. Hamann − *Department of Chemistry, Michigan State University, East Lansing, Michigan 48824, United States;* orcid.org/0000-0001-6917-7494; Email: hamann@chemistry.msu.edu

Jared H. Delcamp − *Department of Chemistry and Biochemistry, University of Mississippi, University, Mississippi 38677, United States;* orcid.org/0000-0001-5313-4078; Email: delcamp@olemiss.edu

Jonah W. Jurss − *Department of Chemistry and Biochemistry, University of Mississippi, University, Mississippi 38677, United States;* orcid.org/0000-0002-2780-3415; Email: jwjurss@olemiss.edu

Authors

Anthony Devdass − *Department of Chemistry and Biochemistry, University of Mississippi, University, Mississippi 38677, United States;* orcid.org/0000-0002-0279-1585

Jonathon Watson − *Department of Chemistry and Biochemistry, University of Mississippi, University, Mississippi 38677, United States;* orcid.org/0000-0003-4307-0730

Eric Firestone − *Department of Chemistry, Michigan State University, East Lansing, Michigan 48824, United States*

Complete contact information is available at: https://pubs.acs.org/10.1021/acsaem.2c00344

Author Contributions

The manuscript was written through contributions of all authors. All authors have given approval to the final version of the manuscript.

Funding

This material is based on work supported by the National Science Foundation under grant no. 1757220 and by the Chemical Sciences, Geosciences, and Biosciences Division, Office of Basic Energy Sciences, Office of Science, the U.S. Department of Energy grant no. DE-SC0017342.

Notes

The authors declare no competing financial interest.

■ ACKNOWLEDGMENTS

We wish to thank Dr. Richard Staples and Dr. Matthias Zeller for crystallographic analysis of the Cu^{II} and Cu^I complexes, respectively, and Dr. Pavel Kucheryavy and Dr. Seonbeom Kim for assisting with variable-temperature ^1H NMR and gradient-selected COSY data collection.

■ REFERENCES

(1) Sachs, J. D. The Road to Clean Energy Starts Here. *Sci. Am.* **2007**, *296*, 39–39.

(2) Bierbaum, R. M.; Matson, P. A. Energy in the Context of Sustainability. *Daedalus* **2013**, *142*, 146–161.

(3) El Chaar, L.; lamont, L. A.; El Zein, N. Review of Photovoltaic Technologies. *Renewable Sustainable Energy Rev.* **2011**, *15*, 2165–2175.

(4) Parida, B.; Iniyan, S.; Goic, R. A Review of Solar Photovoltaic Technologies. *Renewable Sustainable Energy Rev.* **2011**, *15*, 1625–1636.

(5) Hagfeldt, A.; Boschloo, G.; Sun, L.; Kloo, L.; Pettersson, H. Dye-Sensitized Solar Cells. *Chem. Rev.* **2010**, *110*, 6595–6663.

(6) O'Regan, B.; Grätzel, M. A Low-Cost, High-Efficiency Solar Cell Based on Dye-Sensitized Colloidal TiO_2 Films. *Nature* **1991**, *353*, 737–740.

(7) Kakiage, K.; Aoyama, Y.; Yano, T.; Oya, K.; Fujisawa, J.; Hanaya, M. Highly-Efficient Dye-Sensitized Solar Cells with Collaborative Sensitization by Silyl-Anchor and Carboxy-Anchor Dyes. *Chem. Commun.* **2015**, *51*, 15894–15897.

(8) Liu, Q.; Jiang, Y.; Jin, K.; Qin, J.; Xu, J.; Li, W.; Xiong, J.; Liu, J.; Xiao, Z.; Sun, K.; Yang, S.; Zhang, X.; Ding, L. 18% Efficiency Organic Solar Cells. *Sci. Bull.* **2020**, *65*, 272–275.

(9) Freitag, M.; Teuscher, J.; Saygili, Y.; Zhang, X.; Giordano, F.; Liska, P.; Hua, J.; Zakeeruddin, S. M.; Moser, J.-E.; Grätzel, M.; Hagfeldt, A. Dye-Sensitized Solar Cells for Efficient Power Generation under Ambient Lighting. *Nat. Photonics* **2017**, *11*, 372–378.

(10) Cao, Y.; Liu, Y.; Zakeeruddin, S. M.; Hagfeldt, A.; Grätzel, M. Direct Contact of Selective Charge Extraction Layers Enables High-Efficiency Molecular Photovoltaics. *Joule* **2018**, *2*, 1108–1117.

(11) Lu, M. N.; Su, T.-S.; Pylnev, M.; Long, Y.-S.; Wu, T.-C.; Tsai, M.-A.; Wei, T.-C. Stepwise Optimizing Photovoltaic Performance of Dye-Sensitized Cells Made under 50-Lux Dim Light. *Progr. Photovolt.: Res. Appl.* **2021**, *29*, 533−545.
(12) Grätzel, M. Dye-Sensitized Solar Cells. *J. Photochem. Photobiol., C* **2003**, *4*, 145−153.
(13) Sapp, S. A.; Elliott, C. M.; Contado, C.; Caramori, S.; Bignozzi, C. A. Substituted Polypyridine Complexes of Cobalt(II/III) as Efficient Electron-Transfer Mediators in Dye-Sensitized Solar Cells. *J. Am. Chem. Soc.* **2002**, *124*, 11215−11222.
(14) Nusbaumer, H.; Zakeeruddin, S. M.; Moser, J.-E.; Grätzel, M. An Alternative Efficient Redox Couple for the Dye-Sensitized Solar Cell System. *Chem. − Eur. J.* **2003**, *9*, 3756−3763.
(15) Yum, J.-H.; Baranoff, E.; Kessler, F.; Moehl, T.; Ahmad, S.; Bessho, T.; Marchioro, A.; Ghadiri, E.; Moser, J.-E.; Yi, C.; Nazeeruddin, M. K.; Grätzel, M. A Cobalt Complex Redox Shuttle for Dye-Sensitized Solar Cells with High Open-Circuit Potentials. *Nat. Commun.* **2012**, *3*, 631.
(16) Boschloo, G.; Hagfeldt, A. Characteristics of the Iodide/Triiodide Redox Mediator in Dye-Sensitized Solar Cells. *Acc. Chem. Res.* **2009**, *42*, 1819−1826.
(17) Chiba, Y.; Islam, A.; Watanabe, Y.; Komiya, R.; Koide, N.; Han, L. Dye-Sensitized Solar Cells with Conversion Efficiency of 11.1%. *Jpn. J. Appl. Phys.* **2006**, *45*, L638−L640.
(18) Chen, C.-Y.; Wang, M.; Li, J.-Y.; Pootrakulchote, N.; Alibabaei, L.; Ngoc-le, C.; Decoppet, J.-D.; Tsai, J.-H.; Grätzel, C.; Wu, C.-G.; Zakeeruddin, S. M.; Grätzel, M. Highly Efficient Light-Harvesting Ruthenium Sensitizer for Thin-Film Dye-Sensitized Solar Cells. *ACS Nano* **2009**, *3*, 3103−3109.
(19) Xie, Y.; Tang, Y.; Wu, W.; Wang, Y.; Liu, J.; Li, X.; Tian, H.; Zhu, W.-H. Porphyrin Cosensitization for a Photovoltaic Efficiency of 11.5%: A Record for Non-Ruthenium Solar Cells Based on Iodine Electrolyte. *J. Am. Chem. Soc.* **2015**, *137*, 14055−14058.
(20) Ozawa, H.; Sugiura, T.; Kuroda, T.; Nozawa, K.; Arakawa, H. Highly Efficient Dye-Sensitized Solar Cells Based on a Ruthenium Sensitizer Bearing a Hexylthiophene Modified Terpyridine Ligand. *J. Mater. Chem. A* **2016**, *4*, 1762−1770.
(21) Ji, J.-M.; Zhou, H.; Eom, Y. K.; Kim, C. H.; Kim, H. K. 14.2% Efficiency Dye-Sensitized Solar Cells by Co-Sensitizing Novel Thieno[3,2-*b*]Indole-Based Organic Dyes with a Promising Porphyrin Sensitizer. *Adv. Energy Mater.* **2020**, *10*, 2000124.
(22) Green, M. A.; Dunlop, E. D.; Hohl-Ebinger, J.; Yoshita, M.; Kopidakis, N.; Hao, X. Solar Cell Efficiency Tables (Version 56). *Progr. Photovolt.: Res. Appl.* **2020**, *28*, 629−638.
(23) Vlachopoulos, N.; Hagfeldt, A.; Benesperi, I.; Freitag, M.; Hashmi, G.; Jia, G.; Wahyuono, R. A.; Plentz, J.; Dietzek, B. New Approaches in Component Design for Dye-Sensitized Solar Cells. *Sustainable Energy Fuels* **2021**, *5*, 367−383.
(24) Rorabacher, D. B. Electron Transfer by Copper Centers. *Chem. Rev.* **2004**, *104*, 651−698.
(25) Pérez-Henarejos, S. A.; Alcaraz, L. A.; Donaire, A. Blue Copper Proteins: A Rigid Machine for Efficient Electron Transfer, a Flexible Device for Metal Uptake. *Arch. Biochem. Biophys.* **2015**, *584*, 134−148.
(26) Kaim, W.; Rall, J. Copper—A "Modern" Bioelement. *Angew. Chem., Int. Ed.* **1996**, *35*, 43−60.
(27) Hattori, S.; Wada, Y.; Yanagida, S.; Fukuzumi, S. Blue Copper Model Complexes with Distorted Tetragonal Geometry Acting as Effective Electron-Transfer Mediators in Dye-Sensitized Solar Cells. *J. Am. Chem. Soc.* **2005**, *127*, 9648−9654.
(28) Freitag, M.; Daniel, Q.; Pazoki, M.; Sveinbjörnsson, K.; Zhang, J.; Sun, L.; Hagfeldt, A.; Boschloo, G. High-Efficiency Dye-Sensitized Solar Cells with Molecular Copper Phenanthroline as Solid Hole Conductor. *Energy Environ. Sci.* **2015**, *8*, 2634−2637.
(29) Saygili, Y.; Söderberg, M.; Pellet, N.; Giordano, F.; Cao, Y.; Muñoz-García, A. B.; Zakeeruddin, S. M.; Vlachopoulos, N.; Pavone, M.; Boschloo, G.; Kavan, L.; Moser, J.-E.; Grätzel, M.; Hagfeldt, A.; Freitag, M. Copper Bipyridyl Redox Mediators for Dye-Sensitized Solar Cells with High Photovoltage. *J. Am. Chem. Soc.* **2016**, *138*, 15087−15096.
(30) Cong, J.; Kinschel, D.; Daniel, Q.; Safdari, M.; Gabrielsson, E.; Chen, H.; Svensson, P. H.; Sun, L.; Kloo, L. Bis(1,1-Bis(2-Pyridyl)Ethane)Copper(I/II) as an Efficient Redox Couple for Liquid Dye-Sensitized Solar Cells. *J. Mater. Chem. A* **2016**, *4*, 14550−14554.
(31) Magni, M.; Giannuzzi, R.; Colombo, A.; Cipolla, M. P.; Dragonetti, C.; Caramori, S.; Carli, S.; Grisorio, R.; Suranna, G. P.; Bignozzi, C. A.; Roberto, D.; Manca, M. Tetracoordinated Bis-Phenanthroline Copper-Complex Couple as Efficient Redox Mediators for Dye Solar Cells. *Inorg. Chem.* **2016**, *55*, 5245−5253.
(32) Hoffeditz, W. L.; Katz, M. J.; Deria, P.; Cutsail, G. E., III; Pellin, M. J.; Farha, O. K.; Hupp, J. T. One Electron Changes Everything. A Multispecies Copper Redox Shuttle for Dye-Sensitized Solar Cells. *J. Phys. Chem. C* **2016**, *120*, 3731−3740.
(33) Li, J.; Yang, X.; Yu, Z.; Gurzadyan, G. G.; Cheng, M.; Zhang, F.; Cong, J.; Wang, W.; Wang, H.; Li, X.; Kloo, L.; Wang, M.; Sun, L. Efficient Dye-Sensitized Solar Cells with $[Copper(6,6'-Dimethyl-2,2'-Bipyridine)_2]^{2+/1+}$ Redox Shuttle. *RSC Adv.* **2017**, *7*, 4611−4615.
(34) Colombo, A.; Di Carlo, G.; Dragonetti, C.; Magni, M.; Orbelli Biroli, A.; Pizzotti, M.; Roberto, D.; Tessore, F.; Benazzi, E.; Bignozzi, C. A.; Casarin, L.; Caramori, S. Coupling of Zinc Porphyrin Dyes and Copper Electrolytes: A Springboard for Novel Sustainable Dye-Sensitized Solar Cells. *Inorg. Chem.* **2017**, *56*, 14189−14197.
(35) Cao, Y.; Saygili, Y.; Ummadisingu, A.; Teuscher, J.; Luo, J.; Pellet, N.; Giordano, F.; Zakeeruddin, S. M.; Moser, J.-E.; Freitag, M.; Hagfeldt, A.; Grätzel, M. 11% Efficiency Solid-State Dye-Sensitized Solar Cells with Copper(II/I) Hole Transport Materials. *Nat. Commun.* **2017**, *8*, 15390.
(36) García-Rodríguez, R.; Jiang, R.; Canto-Aguilar, E. J.; Oskam, G.; Boschloo, G. Improving the Mass Transport of Copper-Complex Redox Mediators in Dye-Sensitized Solar Cells by Reducing the Inter-Electrode Distance. *Phys. Chem. Chem. Phys.* **2017**, *19*, 32132−32142.
(37) Michaels, H.; Benesperi, I.; Edvinsson, T.; Muñoz-Garcia, A. B.; Pavone, M.; Boschloo, G.; Freitag, M. Copper Complexes with Tetradentate Ligands for Enhanced Charge Transport in Dye-Sensitized Solar Cells. *Inorganics* **2018**, *6*, 53.
(38) Colombo, A.; Ossola, R.; Magni, M.; Roberto, D.; Jacquemin, D.; Castellano, C.; Demartin, F.; Dragonetti, C. Intriguing C−H···Cu Interactions in Bis-(Phenanthroline)Cu(I) Redox Mediators for Dye-Sensitized Solar Cells. *Dalton Trans.* **2018**, *47*, 1018−1022.
(39) Hu, M.; Shen, J.; Yu, Z.; Liao, R.-Z.; Gurzadyan, G. G.; Yang, X.; Hagfeldt, A.; Wang, M.; Sun, L. Efficient and Stable Dye-Sensitized Solar Cells Based on a Tetradentate Copper(II/I) Redox Mediator. *ACS Appl. Mater. Interfaces* **2018**, *10*, 30409−30416.
(40) Pradhan, S. C.; Hagfeldt, A.; Soman, S. Resurgence of DSCs with Copper Electrolyte: A Detailed Investigation of Interfacial Charge Dynamics with Cobalt and Iodine Based Electrolytes. *J. Mater. Chem. A* **2018**, *6*, 22204−22214.
(41) Wang, Y.; Hamann, T. W. Improved Performance Induced by in Situ Ligand Exchange Reactions of Copper Bipyridyl Redox Couples in Dye-Sensitized Solar Cells. *Chem. Commun.* **2018**, *54*, 12361−12364.
(42) Saygili, Y.; Stojanovic, M.; Michaels, H.; Tiepelt, J.; Teuscher, J.; Massaro, A.; Pavone, M.; Giordano, F.; Zakeeruddin, S. M.; Boschloo, G.; Moser, J.-E.; Grätzel, M.; Muñoz-García, A. B.; Hagfeldt, A.; Freitag, M. Effect of Coordination Sphere Geometry of Copper Redox Mediators on Regeneration and Recombination Behavior in Dye-Sensitized Solar Cell Applications. *ACS Appl. Energy Mater.* **2018**, *1*, 4950−4962.
(43) Zhao, Y.; Shen, J.; Yu, Z.; Hu, M.; Liu, C.; Fan, J.; Han, H.; Hagfeldt, A.; Wang, M.; Sun, L. Fine-Tuning the Coordination Atoms of Copper Redox Mediators: An Effective Strategy for Boosting the Photovoltage of Dye-Sensitized Solar Cells. *J. Mater. Chem. A* **2019**, *7*, 12808−12814.
(44) Rodrigues, R. R.; Lee, J. M.; Taylor, N. S.; Cheema, H.; Chen, L.; Fortenberry, R. C.; Delcamp, J. H.; Jurss, J. W. Copper-Based Redox Shuttles Supported by Preorganized Tetradentate Ligands for Dye-Sensitized Solar Cells. *Dalton Trans.* **2020**, *49*, 343−355.

https://doi.org/10.1021/acsaem.2c00344
ACS Appl. Energy Mater. 2022, 5, 5964−5973

(45) Jiang, H.; Ren, Y.; Zhang, W.; Wu, Y.; Socie, E. C.; Carlsen, B. I.; Moser, J.-E.; Tian, H.; Zakeeruddin, S. M.; Zhu, W.-H.; Grätzel, M. Phenanthrene-Fused-Quinoxaline as a Key Building Block for Highly Efficient and Stable Sensitizers in Copper-Electrolyte-Based Dye-Sensitized Solar Cells. *Angew. Chem., Int. Ed.* **2020**, *59*, 9324−9329.
(46) Glinka, A.; Gierszewski, M.; Gierczyk, B.; Burdziński, G.; Michaels, H.; Freitag, M.; Ziółek, M. Interface Modification and Exceptionally Fast Regeneration in Copper Mediated Solar Cells Sensitized with Indoline Dyes. *J. Phys. Chem. C* **2020**, *124*, 2895−2906.
(47) Higashino, T.; Iiyama, H.; Nishimura, I.; Imahori, H. Exploration on the Combination of Push-Pull Porphyrin Dyes and Copper(I/II) Redox Shuttles toward High-Performance Dye-Sensitized Solar Cells. *Chem. Lett.* **2020**, *49*, 936−939.
(48) Higashino, T.; Iiyama, H.; Nimura, S.; Kurumisawa, Y.; Imahori, H. Effect of Ligand Structures of Copper Redox Shuttles on Photovoltaic Performance of Dye-Sensitized Solar Cells. *Inorg. Chem.* **2020**, *59*, 452−459.
(49) Ren, Y.; Flores-Díaz, N.; Zhang, D.; Cao, Y.; Decoppet, J.-D.; Fish, G. C.; Moser, J.-E.; Zakeeruddin, S. M.; Wang, P.; Hagfeldt, A.; Grätzel, M. Blue Photosensitizer with Copper(II/I) Redox Mediator for Efficient and Stable Dye-Sensitized Solar Cells. *Adv. Funct. Mater.* **2020**, *30*, 2004804.
(50) Michaels, H.; Rinderle, M.; Freitag, R.; Benesperi, I.; Edvinsson, T.; Socher, R.; Gagliardi, A.; Freitag, M. Dye-Sensitized Solar Cells under Ambient Light Powering Machine Learning: Towards Autonomous Smart Sensors for the Internet of Things. *Chem. Sci.* **2020**, *11*, 2895−2906.
(51) Yoo, K.; Biswas, S.; Lee, Y.-J.; Shin, S.-C.; Kim, K.-J.; Shim, J. W.; Kim, H.; Lee, J.-J. Standardizing Performance Measurement of Dye-Sensitized Solar Cells for Indoor Light Harvesting. *IEEE Access* **2020**, *8*, 114752−114760.
(52) Zheng, H.; Li, D.; Ran, C.; Zhong, Q.; Song, L.; Chen, Y.; Müller-Buschbaum, P.; Huang, W. Emerging Organic/Hybrid Photovoltaic Cells for Indoor Applications: Recent Advances and Perspectives. *Solar RRL* **2021**, *5*, 2100042.
(53) Zhang, D.; Stojanovic, M.; Ren, Y.; Cao, Y.; Eickemeyer, F. T.; Socie, E.; Vlachopoulos, N.; Moser, J.-E.; Zakeeruddin, S. M.; Hagfeldt, A.; Grätzel, M. A Molecular Photosensitizer Achieves a V_{OC} of 1.24 V Enabling Highly Efficient and Stable Dye-Sensitized Solar Cells with Copper(II/I)-Based Electrolyte. *Nat. Commun.* **2021**, *12*, 1777.
(54) Feldt, S. M.; Wang, G.; Boschloo, G.; Hagfeldt, A. Effects of Driving Forces for Recombination and Regeneration on the Photovoltaic Performance of Dye-Sensitized Solar Cells Using Cobalt Polypyridine Redox Couples. *J. Phys. Chem. C* **2011**, *115*, 21500−21507.
(55) Mosconi, E.; Yum, J.-H.; Kessler, F.; Gómez García, C. J.; Zuccaccia, C.; Cinti, A.; Nazeeruddin, M. K.; Grätzel, M.; De Angelis, F. Cobalt Electrolyte/Dye Interactions in Dye-Sensitized Solar Cells: A Combined Computational and Experimental Study. *J. Am. Chem. Soc.* **2012**, *134*, 19438−19453.
(56) Yang, K.; Yang, X.; Zhang, L.; An, J.; Wang, H.; Deng, Z. Copper Redox Mediators with Alkoxy Groups Suppressing Recombination for Dye-Sensitized Solar Cells. *Electrochim. Acta* **2021**, *368*, 137564.
(57) Birker, P. J. M. W. L.; Helder, J.; Henkel, G.; Krebs, B.; Reedijk, J. Synthesis and Spectroscopic Characterization of Copper(I) and Copper(II) Complexes with 1,6-Bis(2-Benzimidazolyl)-2,5-Dithiahexane (BBDH). X-Ray Structure of Trigonal-Bipyramidal Coordinated $[Cu(BBDH)Cl]Cl{\bullet}2C_2H_5OH$. *Inorg. Chem.* **1982**, *21*, 357−363.
(58) Rui, H.; Shen, J.; Yu, Z.; Li, L.; Han, H.; Sun, L. Stable Dye-Sensitized Solar Cells Based on Copper(II/I) Redox Mediators Bearing a Pentadentate Ligand. *Angew. Chem., Int. Ed.* **2021**, *60*, 16156−16163.
(59) Kashif, M. K.; Nippe, M.; Duffy, N. W.; Forsyth, C. M.; Chang, C. J.; Long, J. R.; Spiccia, L.; Bach, U. Stable Dye-Sensitized Solar Cell Electrolytes Based on Cobalt(II)/(III) Complexes of a Hexadentate Pyridyl Ligand. *Angew. Chem., Int. Ed.* **2013**, *52*, 5527−5531.
(60) Bechlars, B.; D'Alessandro, D. M.; Jenkins, D. M.; Iavarone, A. T.; Glover, S. D.; Kubiak, C. P.; Long, J. R. High-Spin Ground States via Electron Delocalization in Mixed-Valence Imidazolate-Bridged Divanadium Complexes. *Nat. Chem.* **2010**, *2*, 362−368.
(61) Kamata, K.; Suzuki, A.; Nakai, Y.; Nakazawa, H. Catalytic Hydrosilylation of Alkenes by Iron Complexes Containing Terpyridine Derivatives as Ancillary Ligands. *Organometallics* **2012**, *31*, 3825−3828.
(62) Addison, A. W.; Burke, P. J.; Henrick, K.; Rao, T. N.; Sinn, E. Pentacoordinate Copper Complexes of Nitrogen-Sulfur Donors: Structural Chemistry of Two Complexes of Bis(2-(2-Benzimidazolyl)-Ethyl) Sulfide with the Sulfur Alternatively in Equatorial and Axial Coordination Modes. *Inorg. Chem.* **1983**, *22*, 3645−3653.
(63) Yang, L.; Powell, D. R.; Houser, R. P. Structural Variation in Copper(I) Complexes with Pyridylmethylamide Ligands: Structural Analysis with a New Four-Coordinate Geometry Index, T4. *Dalton Trans.* **2007**, 955−964.
(64) Niu, J.; Zhou, H.; Li, Z.; Xu, J.; Hu, S. An Efficient Ullmann-Type C−O Bond Formation Catalyzed by an Air-Stable Copper(I)−Bipyridyl Complex. *J. Org. Chem.* **2008**, *73*, 7814−7817.
(65) Linfoot, C. L.; Richardson, P.; Hewat, T. E.; Moudam, O.; Forde, M. M.; Collins, A.; White, F.; Robertson, N. Substituted [Cu(I)(POP)(Bipyridyl)] and Related Complexes: Synthesis, Structure, Properties and Applications to Dye-Sensitised Solar Cells. *Dalton Trans.* **2010**, *39*, 8945−8956.
(66) Bozic-Weber, B.; Chaurin, V.; Constable, E. C.; Housecroft, C. E.; Meuwly, M.; Neuburger, M.; Rudd, J. A.; Schönhofer, E.; Siegfried, L. Exploring Copper(I)-Based Dye-Sensitized Solar Cells: A Complementary Experimental and TD-DFT Investigation. *Dalton Trans.* **2012**, *41*, 14157−14169.
(67) Zimmer, K. D.; Shoemaker, R.; Ruminski, R. R. Synthesis and Characterization of a Fluxional Re(I) Carbonyl Complex *fac*-$[Re(CO)_3(Dpop')Cl]$ with the Nominally Tri-Dentate Ligand Dipyrido(2,3-*a*:3′,2′-*j*)Phenazine (Dpop′). *Inorg. Chim. Acta* **2006**, *359*, 1478−1484.
(68) Zhang, J.; Siu, K.; Lin, C. H.; Canary, J. W. Conformational Dynamics of Cu(i) Complexes of Tripodal Ligands: Steric Control of Molecular Motion. *New J. Chem.* **2005**, *29*, 1147.
(69) Karlin, K. D.; Hayes, J. C.; Juen, S.; Hutchinson, J. P.; Zubieta, J. Tetragonal vs. Trigonal Coordination in Copper(II) Complexes with Tripod Ligands: Structures and Properties of $[Cu(C_{21}H_{24}N_4)Cl]PF_6$ and $[Cu(C_{18}H_{18}N_4)Cl]PF_6$. *Inorg. Chem.* **1982**, *21*, 4106−4108.
(70) Mautner, F. A.; Vicente, R.; Massoud, S. S. Structure Determination of Nitrito- and Thiocyanato-Copper(II) Complexes: X-ray Structures of $[Cu(Medpt)(ONO)(H_2O)]ClO_4$ (1), $[Cu(dien)(ONO)]ClO_4$ (2) and $[Cu_2(Medpt)_2(\mu_{N,S}\text{-}NCS)_2](ClO_4)_2$ (3) (Medpt = 3,3′-Diamino-*N*-Methyldipropylamine and dien=diethylenetriamine). *Polyhedron* **2006**, *25*, 1673−1680.
(71) Schatz, M.; Becker, M.; Thaler, F.; Hampel, F.; Schindler, S.; Jacobson, R. R.; Tyeklár, Z.; Murthy, N. N.; Ghosh, P.; Chen, Q.; Zubieta, J.; Karlin, K. D. Copper(I) Complexes, Copper(I)/O_2 Reactivity, and Copper(II) Complex Adducts, with a Series of Tetradentate Tripyridylalkylamine Tripodal Ligands. *Inorg. Chem.* **2001**, *40*, 2312−2322.
(72) Devdass, A.; Talukdar, K.; Zeller, M.; Fortenberry, R. C.; Jurss, J. W. Exploring Different Equatorial Donors in a Series of Five-Coordinate Cu(II) Complexes Supported by Rigid Tetradentate Ligands. *Polyhedron* **2022**, No. 115558.
(73) Connelly, N. G.; Geiger, W. E. Chemical Redox Agents for Organometallic Chemistry. *Chem. Rev.* **1996**, *96*, 877−910.
(74) Weast, R. C.; Astle, M. J. *CRC Handbook of Chemistry and Physics : A Ready-Reference Book of Chemical and Physical Data*; The CRC Press: Boca Raton, Fla., 1982.
(75) Ambundo, E. A.; Deydier, M.-V.; Grall, A. J.; Aguera-Vega, N.; Dressel, L. T.; Cooper, T. H.; Heeg, M. J.; Ochrymowycz, L. A.; Rorabacher, D. B. Influence of Coordination Geometry upon Copper(II/I) Redox Potentials. Physical Parameters for Twelve

https://doi.org/10.1021/acsaem.2c00344
ACS Appl. Energy Mater. 2022, 5, 5964−5973

Copper Tripodal Ligand Complexes. *Inorg. Chem.* **1999**, *38*, 4233−4242.
(76) Kusama, H.; Konishi, Y.; Sugihara, H.; Arakawa, H. Influence of Alkylpyridine Additives in Electrolyte Solution on the Performance of Dye-Sensitized Solar Cell. *Sol. Energy Mater. Sol. Cells* **2003**, *80*, 167−179.
(77) Nakade, S.; Kanzaki, T.; Kubo, W.; Kitamura, T.; Wada, Y.; Yanagida, S. Role of Electrolytes on Charge Recombination in Dye-Sensitized TiO_2 Solar Cell (1): The Case of Solar Cells Using the I-/I_3- Redox Couple. *J. Phys. Chem. B* **2005**, *109*, 3480−3487.
(78) Kashif, M. K.; Axelson, J. C.; Duffy, N. W.; Forsyth, C. M.; Chang, C. J.; Long, J. R.; Spiccia, L.; Bach, U. A New Direction in Dye-Sensitized Solar Cells Redox Mediator Development: In Situ Fine-Tuning of the Cobalt(II)/(III) Redox Potential through Lewis Base Interactions. *J. Am. Chem. Soc.* **2012**, *134*, 16646−16653.
(79) Boschloo, G.; Häggman, L.; Hagfeldt, A. Quantification of the Effect of 4-*Tert*-Butylpyridine Addition to I^-/I_3^- Redox Electrolytes in Dye-Sensitized Nanostructured TiO_2 Solar Cells. *J. Phys. Chem. B* **2006**, *110*, 13144−13150.
(80) Koops, S. E.; O'Regan, B. C.; Barnes, P. R. F.; Durrant, J. R. Parameters Influencing the Efficiency of Electron Injection in Dye-Sensitized Solar Cells. *J. Am. Chem. Soc.* **2009**, *131*, 4808−4818.
(81) Long, H.; Zhou, D.; Zhang, M.; Peng, C.; Uchida, S.; Wang, P. Probing Dye-Correlated Interplay of Energetics and Kinetics in Mesoscopic Titania Solar Cells with 4-Tert-Butylpyridine. *J. Phys. Chem. C* **2011**, *115*, 14408−14414.
(82) Fürer, S. O.; Milhuisen, R. A.; Kashif, M. K.; Raga, S. R.; Acharya, S. S.; Forsyth, C.; Liu, M.; Frazer, L.; Duffy, N. W.; Ohlin, C. A.; Funston, A. M.; Tachibana, Y.; Bach, U. The Performance-Determining Role of Lewis Bases in Dye-Sensitized Solar Cells Employing Copper-Bisphenanthroline Redox Mediators. *Adv. Energy Mater.* **2020**, *10*, 2002067.
(83) Kannankutty, K.; Chen, C.-C.; Nguyen, V. S.; Lin, Y.-C.; Chou, H.-H.; Yeh, C.-Y.; Wei, T.-C. Tert-Butylpyridine Coordination with $[Cu(dmp)_2]^{2+/+}$ Redox Couple and Its Connection to the Stability of the Dye-Sensitized Solar Cell. *ACS Appl. Mater. Interfaces* **2020**, *12*, 5812−5819.
(84) Kavan, L.; Saygili, Y.; Freitag, M.; Zakeeruddin, S. M.; Hagfeldt, A.; Grätzel, M. Electrochemical Properties of Cu(II/I)-Based Redox Mediators for Dye-Sensitized Solar Cells. *Electrochim. Acta* **2017**, *227*, 194−202.
(85) Deng, Z.; Yang, X.; Yang, K.; Zhang, L.; Wang, H.; Wang, X.; Sun, L. Helical Copper Redox Mediator with Low Electron Recombination for Dye-Sensitized Solar Cells. *ACS Sustainable Chem. Eng.* **2021**, *9*, 5252−5259.
(86) Giordano, M.; Volpi, G.; Bonomo, M.; Mariani, P.; Garino, C.; Viscardi, G. Methoxy-Substituted Copper Complexes as Possible Redox Mediators in Dye-Sensitized Solar Cells. *New J. Chem.* **2021**, *45*, 15303−15311.
(87) Xie, Y.; Baillargeon, J.; Hamann, T. W. Kinetics of Regeneration and Recombination Reactions in Dye-Sensitized Solar Cells Employing Cobalt Redox Shuttles. *J. Phys. Chem. C* **2015**, *119*, 28155−28166.
(88) Royea, W. J.; Hamann, T. W.; Brunschwig, B. S.; Lewis, N. S. A Comparison between Interfacial Electron-Transfer Rate Constants at Metallic and Graphite Electrodes. *J. Phys. Chem. B* **2006**, *110*, 19433−19442.
(89) Curiac, C.; Rodrigues, R. R.; Watson, J.; Hunt, L. A.; Devdass, A.; Jurss, J. W.; Hammer, N. I.; Fortenberry, R. C.; Delcamp, J. H. Iron Redox Shuttles with Wide Optical Gap Dyes for High-Voltage Dye-Sensitized Solar Cells. *ChemSusChem* **2021**, *14*, 3084−3096.
(90) Anderson, A. Y.; Barnes, P. R. F.; Durrant, J. R.; O'Regan, B. C. Quantifying Regeneration in Dye-Sensitized Solar Cells. *J. Phys. Chem. C* **2011**, *115*, 2439−2447.
(91) Ronca, E.; Pastore, M.; Belpassi, L.; Tarantelli, F.; Angelis, F. D. Influence of the Dye Molecular Structure on the TiO_2 Conduction Band in Dye-Sensitized Solar Cells: Disentangling Charge Transfer and Electrostatic Effects. *Energy Environ. Sci.* **2013**, *6*, 183−193.
(92) Srivishnu, K. S.; Prasanthkumar, S.; Giribabu, L. Cu(II/I) Redox Couples: Potential Alternatives to Traditional Electrolytes for Dye-Sensitized Solar Cells. *Mater. Adv.* **2021**, *2*, 1229−1247.
(93) Kim, T.-Y.; Wang, Y.; Raithel, A. L.; Hamann, T. W. Real-Time Observation of the Diffusion Mechanism Progression from Liquid to Solid State of Transition Metal Complexes. *ACS Energy Lett.* **2020**, *5*, 583−588.
(94) Bruker, S. V. A. *APEX3 V2016.9−0, SAINT V8.37A*; Bruker AXS Inc.: Madison (WI), USA, 2013/2014.
(95) Sheldrick, G. M. A Short History of SHELX. *Acta Crystallogr., Sect. A: Found. Crystallogr.* **2008**, *64*, 112−122.
(96) V. SHELXTL *Suits of Programs, 2000−2003;* Bruker Advanced X-Ray Solutions: Bruker AXS Inc.: Madison (WI), USA.
(97) Sheldrick, G. M. Crystal Structure Refinement with SHELXL. *Acta Crystallogr., Sect. C: Struct. Chem.* **2015**, *71*, 3−8.
(98) Sheldrick, G. M. *Shelxl2018*; University of Göttingen, 2018.
(99) Hübschle, C. B.; Sheldrick, G. M.; Dittrich, B. ShelXle: A Qt Graphical User Interface for SHELXL. *J. Appl. Crystallogr.* **2011**, *44*, 1281−1284.
(100) Cheema, H.; Delcamp, J. H. SnO_2 Transparent Printing Pastes from Powders for Photon Conversion in SnO_2-Based Dye-Sensitized Solar Cells. *Chem. − Eur. J.* **2019**, *25*, 14205−14213.
(101) Ellis, H.; Vlachopoulos, N.; Häggman, L.; Perruchot, C.; Jouini, M.; Boschloo, G.; Hagfeldt, A. PEDOT Counter Electrodes for Dye-Sensitized Solar Cells Prepared by Aqueous Micellar Electrodeposition. *Electrochim. Acta* **2013**, *107*, 45−51.

https://doi.org/10.1021/acsaem.2c00344
ACS Appl. Energy Mater. 2022, 5, 5964−5973